Oscillatory Viscoelastic Microfluidics for Efficient Focusing and Separation of Nanoscale Species

Mohammad Asghari,[†] Xiaobao Cao,[†] Bogdan Mateescu,[‡] Daniel van Leeuwen,[‡] Mahmut Kamil Aslan,[†] Stavros Stavrakis,*,[†] and Andrew J. deMello*,[†]

[†]Institute for Chemical and Bioengineering, ETH Zürich, Vladimir Prelog Weg 1, 8093 Zürich, Switzerland
[‡]Department of Biology, ETH Zürich, Universitätstrasse 2, 8092 Zürich, Switzerland

S *Supporting Information*

ABSTRACT: The ability to precisely control particle migration within microfluidic systems is essential for focusing, separating, counting, and detecting a wide range of biological species. To date, viscoelastic microfluidic systems have primarily been applied to the focusing, separation, and isolation of micrometer-sized species, with their use in nanoparticle manipulations being underdeveloped and underexplored, due to issues related to nanoparticle diffusivity and a need for extended channel lengths. To overcome such issues, we herein present

sheathless oscillatory viscoelastic microfluidics as a method for focusing and separating both micrometer and submicrometer species. To highlight the efficacy of our approach, we segment our study into three size regimes, namely, micrometer (where characteristic particle dimensions are above 1 μm), sub-micrometer (where characteristic dimensions are between 1 μm and 100 nm), and nano (where characteristic dimensions are below 100 nm) regimes. Based on the ability to successfully manipulate particles in all these regimes, we demonstrate the successful isolation of p-bodies from biofluids (in the micrometer regime), the focusing of λ-DNA (in the sub-micrometer regime), and the focusing of extracellular vesicles (in the nanoregime). Finally, we characterize the physics underlying viscoelastic microflows using a dimensionless number that relates the lateral velocity (due to elastic effects) to the diffusion constant of the species within the viscoelastic carrier fluid. Based on the ability to precisely manipulate species in all three regimes, we expect that sheathless oscillatory viscoelastic microfluidics may be used to good effect in a range of biological and life science applications.

KEYWORDS: *viscoelastic microfluidics, extracellular vesicles, oscillatory flow, exosomes, Brownian motion*
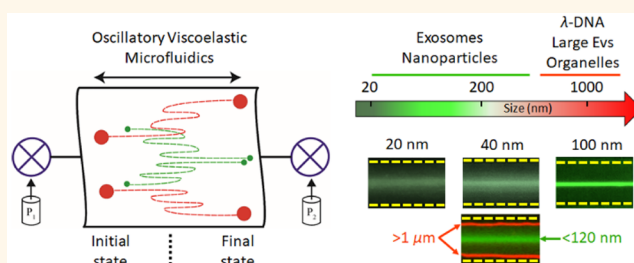
In recent years, much attention has focused on the characterization of circulating particles within biofluids,[1] with a view to improving the sensitivity and specificity of biomarker detection strategies.[2,3] For example, small extracellular vesicles (sEVs) have diameters between 80 and 300 nm and are known to circulate within a variety of biofluids. sEVs exhibit protein, DNA, and RNA profiles that are modulated during cancer progression and therapy, and thus can be used for noninvasive monitoring of disease progression based on their molecular profile.[1,4,5] Unsurprisingly, a number of techniques have been developed to selectively isolate such species from other circulating debris and cells within biofluids. These include methods based on differential centrifugation,[6,7] density gradient separation,[8] affinity capture,[9] size-exclusion chromatography,[10] and ultrafiltration[11] or a combination of these,[12] which fractionate particle diversity on the basis of size, density, and surface markers. However, it is important to note

that these approaches are cumbersome, low throughput in nature, and expensive and require significant volumes of biofluid, thus limiting their routine application in clinical or diagnostic settings. To address many of these limitations, flow-cytometry-based strategies have been developed to allow for efficient sorting of bioparticles based on size and/or surface markers using reduced sample volumes.[13] However, sorting rates are limited by the relatively low sample concentrations (necessary to avoid swarming effects), and the resolution of sEVs below 500 nm requires the adoption of fluorescent labeling strategies.[14,15]

Recently, microfluidic systems have emerged as promising tools for the fast, efficient, and robust focusing and isolation of

micrometer-sized species from biofluids. Indeed, a variety of microfluidic techniques have already been shown to be effective for such purposes. Based on the manipulating forces involved, these methods can be categorized as being either active or passive in nature. Active techniques such as dielectrophoresis (DEP),[16,17] magnetophoresis (MP),[18] and acoustophoresis (AP)[19,20] rely on the application of an external force field, whereas passive techniques solely rely on the control of geometrical and fluid properties (*i.e.*, intrinsic hydrodynamic forces), such as pinched flow fractionation (PFF),[21] deterministic lateral displacement (DLD),[22,23] and inertial microfluidics.[24] Among passive approaches, inertial microfluidic systems have attracted the most attention due to their ability to process biofluids at extremely high volumetric flow rates (~mL/min), which is especially useful in rare event detection applications, such as the isolation of circulating tumor cells (CTCs).[26] In the case of inertial focusing, particles of a given size are transported along a microchannel and preferentially migrate to well-defined positions across the channel cross-section.[24,25] Such inertial approaches are well suited to label-free and high-throughput manipulation of microparticles and cells. Despite the robustness of inertial focusing in Newtonian fluids, its practical implementation for the isolation of nanoscale species has been limited, primarily due to the increasing role of Brownian motion as particle size decreases. To this end, elastic forces (stemming from the rheological properties of the processing fluid) can in principle be used to provide for enhanced control over species with sub-micrometer dimensions.

Viscoelastic manipulation of micrometer-sized particles within microfluidic channels has been used to good effect in both focusing and sorting applications. In basic terms, viscoelastic fluids exhibit both viscous and elastic characteristics when undergoing deformation. Such behavior creates a normal stress anisotropy within the fluid, which leads to transverse forces and lateral migration of particles inside the medium. Karnis et al. first reported viscoelasticity-induced lateral migration of noncolloidal, buoyancy-free particles toward the flow axis in macroscale pipes.[27] In subsequent studies, Leal et al.[28] and Brunn[29] derived models for the lateral migration velocity of rigid spheres in second-order fluids, noting that the ratio of the lateral and longitudinal velocities scales with the square of the blockage ratio. Importantly, such analyses suggest a need for extended channel/pipe lengths when focusing micrometer-sized particles to well-defined positions and highlight the potential of viscoelastic microfluidics for the precise confinement of particles due to the accessibility of high blockage ratios within microchannels.[29] Accordingly, viscoelastic microfluidic systems have been used in a variety of particle focusing, separation, and flow cytometry studies.[30−42] For example, D'Avino and co-workers demonstrated through both numerical simulations and experiment that small blockage ratios result in inward migration of particles toward the centerline, whereas high blockage ratios favor wall attraction.[30] In addition, by implementing a non-Newtonian sheath flow, both size-[38] and shape-based[39] particle separations have been demonstrated. Most recently, CTC isolation from untreated whole blood has been demonstrated using a non-Newtonian fluid sheath flow.[43] Based on the intrinsic elastic properties of viscoelastic fluids, the need for externally imposed force fields or complex channels geometries (typical in inertial systems) is eliminated, and thus viscoelastic microfluidic systems normally comprise simple straight micro-

channels.[44−47] Indeed, Kang *et al.* showed that an extremely dilute solution of λ-DNA can be used to confine micrometer-diameter particles at the center of a straight microtube due to its superior elastic properties when compared to synthetic polymer solutions.[44] Furthermore, sheathless shape-based (spherical and peanut shaped) and size-based (spherical) microparticle sorting has been demonstrated using viscoelastic fluids.[48,49]

Although, many of the above studies have been successful in manipulating micrometer-sized objects, the focusing and separation of sub-micrometer species is far more challenging due to the fact that the elastic force scales with particle volume. That said, Kim *et al.* recently reported for the first time the use of viscoelastic fluids to focus 500 and 200 nm particles along a straight microfluidic channel, although no significant focusing was observed for 100 nm particles.[50] Related studies also demonstrated that 200 nm particles could be focused at the center of an 8 cm long cylindrical microchannel by adjusting flow rates so that elastic forces dominate Brownian forces.[51] Additionally, Liu and co-workers used a double spiral channel (with a total length exceeding 6 cm) to focus and efficiently separate two sets of binary mixtures, namely, 100/2000 nm polystyrene particles and λ-DNA molecules/platelets.[52] Subsequently, the same group used a viscoelastic-based method incorporating a non-Newtonian sheath fluid to isolate exosomes from serum in a continuous manner.[53] Despite these successes, all the aforementioned studies required the use of channel lengths on the order of a few centimeters for the focusing of sub-micrometer particles.[52] Moreover, the processing of species with characteristic dimensions less than 100 nm is even more challenging due to the effects of Brownian forces on smaller nanoparticles, leading to the use of high pressures within extended channels.

Recently, oscillatory flows have been used to eliminate the need for long microchannel lengths and successfully applied to the inertial ordering[54] and focusing of particles down to 500 nm.[55] However, the use of oscillatory flows to manipulate species below this size is still unexplored. Mutlu *et al.* have demonstrated that oscillatory inertial microfluidics can be used to focus particles in low Reynolds number regimes (1 order of magnitude less than steady-flow inertial microfluidics).[55] However, the efficient focusing of species with dimensions below 100 nm would require microchannels with reduced dimensional cross-sections and channel lengths (on the order of a few millimeters or micrometers) to allow access to high flow velocities. Although, such structures have been fabricated in rigid epoxy[46] or silicon[56] for example, system complexity and cost are unavoidably increased.

To this end, herein we present an oscillatory viscoelastic system, incorporating a sheath-free microchannel that is able to focus and separate particles and biological species with diameters ranging from a few micrometers to a few tens of nanometers. Figure 1a shows a schematic view of the microfluidic platform, which includes a pressure-driven microfluidic chip coupled with an in-house electronic circuit to generate oscillatory flow. Using such an approach, objects oscillating within the microfluidic channel can be focused at specific locations based on their size (Figure 1b). Specifically, we initially focus and separate 10, 5, and 1 μm diameter particles within a short (4 mm long) microchannel. The same geometry is then used to separate and process RNA granules (p-bodies) from a mammalian cell lysate sample. Subsequently, oscillatory viscoelastic flows are used to perform rapid and
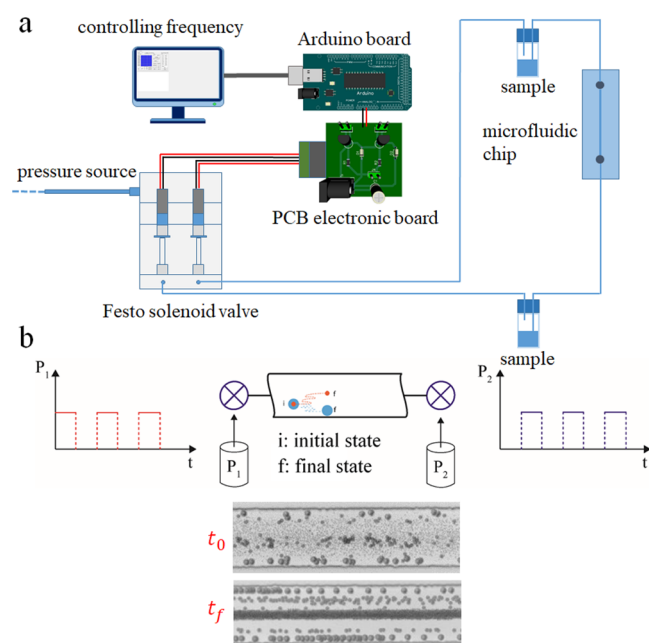
Figure 1. Principal of the oscillatory viscoelastic microfluidics. (a) Schematic of the oscillatory viscoelastic microfluidic setup. The system consists of solenoid valves (Festo, Zuirch, Switzerland) which are connected to a pressure source and an electronic PCB board responsible for actuating the valves to open and close states. A custom-made software is used to control the frequency and the number of oscillations. (b) Oscillatory flow is generated by using the system described in part (a), and elastic forces acting on the particles cause the lateral migration and eventually focusing of them. Particles of different size (1, 5, and 10 μm) with a randomly distributed initial position (t_0) can be focused at discrete parts of the microchannel after a sufficient number of oscillations (t_f).

efficient single-file focusing of 500, 200, and 100 nm diameter nanoparticles along a short-length high aspect ratio microchannel. Finally, and for the first time, focusing of 40 and 20 nm diameter particles is demonstrated. The combination of viscoelastic microfluidics and oscillatory flows is shown to be highly effective in overcoming Brownian motion and is widely applicable to the precise focusing of objects with sizes as small as 20 nm. Given the performance of our experimental setup (using artificial particles), we explored the potential of oscillatory viscoelastic microfluidics in manipulating biological species and demonstrate efficient focusing of both λ-DNA and small extracellular vesicles (<200 nm).

RESULTS AND DISCUSSION

Viscoelastic Microparticle Focusing and Separation Based on Oscillatory Flow. To examine the capabilities of oscillatory viscoelastic flows for separating micrometer-sized species, a ternary mixture of particles, with average diameters of 10, 5, and 1 μm, was introduced in the microfluidic device. The effect of pressure (controlling both elasticity and inertia effect) on particle migration was studied for pressures between 1 and 2.5 bar (in 0.5 bar steps) and an oscillation frequency of 2 Hz, with particles being allowed to reach steady state positions before final images were taken. As shown in Figure 2a, a pressure increase results in an increase in both inertia and elasticity (defined by the Reynolds number, Re, and Weissenberg number, Wi, respectively: Supplementary Note 1). Since the highest Re accessed is 0.08 (indicating negligible

effects of inertia), the driver for the lateral migration of particles is the elasticity-induced lift force. Within an oscillation period of a few seconds, 10 μm diameter particles focus near the microchannel walls and 5 μm diameter particles between the centerline and walls, with 1 μm particles being aligned to the microchannel centerline. The reason for such a migration behavior can be understood through consideration of the blockage ratio, $\beta = a_p/D_h$, where a_p reports the particle size and D_h is the hydraulic diameter of the microchannel. Herein, a higher blockage ratio leads to a greater off-center shift of the viscoelastic focusing positions.

Such behavior implies that two opposing elastic forces affect lateral migration, *i.e.*, a centerline-directed elastic force, $F_{el \to c}$, and a wall-directed elastic force $F_{el \to w}$.[49] Competition between the two components of the elastic lift force determines the lateral focusing position of particles on the basis of their size and flow rate. Based on the results shown in Figure 2, smaller particles (having a low blockage ratio) tend to focus at the centerline due to the dominance of $F_{el \to c}$ over $F_{el \to w}$.[49] On the other hand, since $F_{el \to w}$ is more strongly dependent on the particle size than $F_{el \to c}$,[49] larger particles (having high blockage ratios) tend to migrate to off-center focusing positions due to stronger wall-directed elastic forces ($F_{el \to w}$). As shown in Figure 2a, the highest focusing efficiency takes place when Wi = 1.3 and Re = 0.03. An increase in pressure (Re = 0.03 to 0.08 and Wi = 1.3 to 3.25) causes larger particles to migrate toward the centerline, with smaller particles diverging from it.

Figure 2b presents the time evolution of oscillatory focusing and separation of the particles for the case when Wi = 1.3 and Re = 0.03 (see Supplementary Movie S1). All plots were extracted from the expansion part of the microchannel, and acquisition commenced after 100 ms, *i.e.*, when particles have already traveled a distance of 2 mm from the inlet. Even after such a short period of time, the 10-μm-diameter particles have already started to migrate toward the microchannel walls and 5 μm particles have been depleted from the center and are accumulating in a semifocused state, with the 1 μm particles being dispersed across the expansion zone. After 4 s of oscillation, all particles have reached their final equilibrium positions and have traveled an effective distance of 76 800 μm, a sufficient length to ensure complete separation (Supplementary Movie S2).

As a further proof that the oscillatory focusing platform is capable of separating micrometer-sized species over short path lengths, we then applied this method to a complex and relevant biological sample. Specifically, we attempted to purify p-bodies, cytoplasmic RNA granules that are involved in RNA metabolism and have sizes ranging from 300 nm to 1 μm.[57] For this purpose, we introduced lysate from cells expressing mNG-AGO2 (AGO2 being known to be enriched in p-bodies)[58] into the oscillatory system. The lysate contains nuclei (~6 μm in size), debris, and organelles, including p-bodies (~1 μm in size) that are stable in the lysis solution. Since biological particles are significantly more deformable than rigid particles, a 0.5% PEO polymer solution was used (to decrease elastic effects). As shown in Figure 2c (bright-field image), nuclei and large organelles are concentrated near the walls, in a similar manner to large, rigid particles, since their size is comparable to the channel height, while p-bodies and smaller organelles are focused at the centerline of the channel. This is further demonstrated by the observation of fluorescently mNG-labeled p-bodies at the center outlet (fluorescence image in Figure 2c). Indeed, in a similar manner
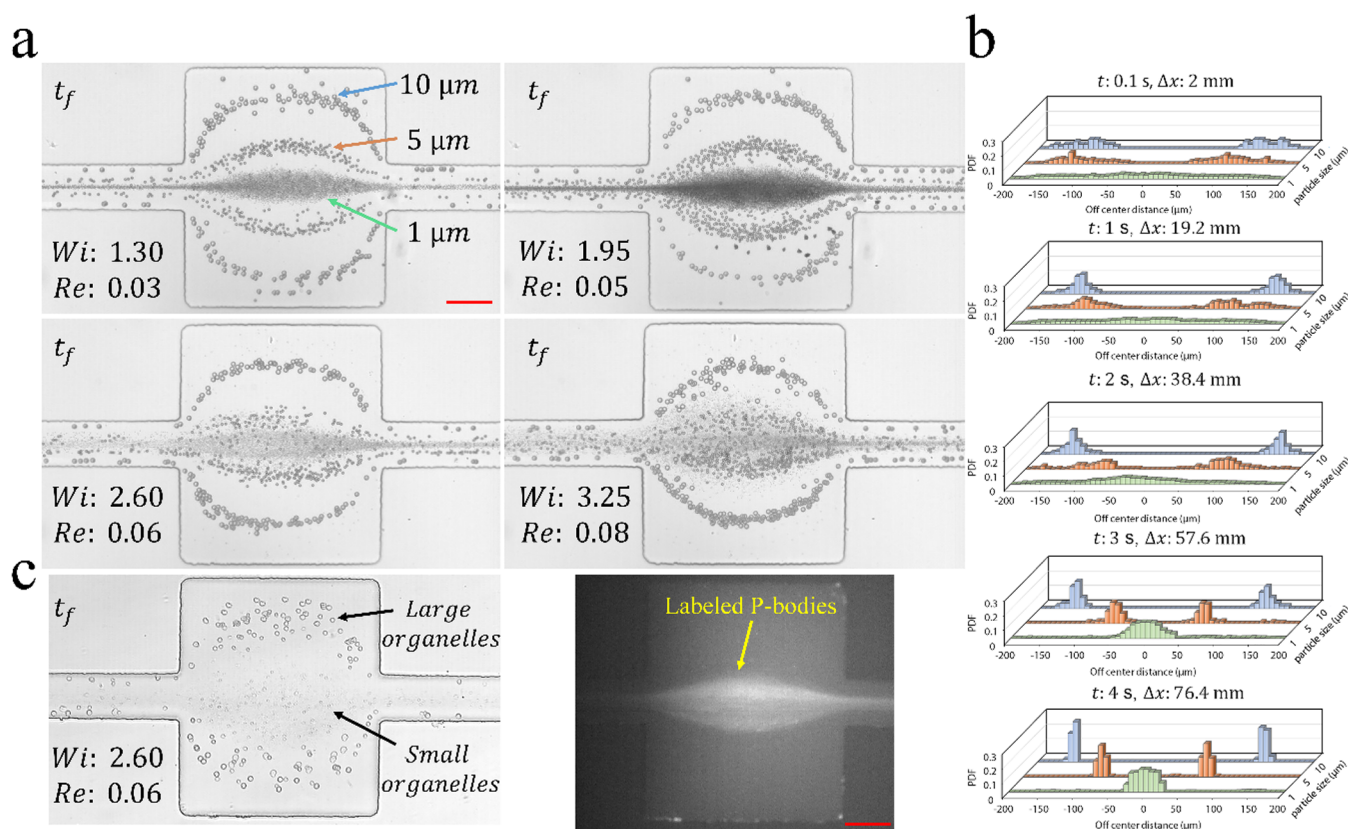
Figure 2. PS microparticle and bioparticle focusing and separation using oscillatory viscoelastic microfluidics. (a) Effect of pressure (in terms of Wi and Re) on the focusing and separation of 1, 5, and 10 μm particles in PEO$_{600kDa,1\%}$, in a straight 80 μm width, 12 μm height, and 4 mm length microchannel with an oscillating frequency of 2 Hz. An expansion area with 400 μm width and 12 μm height at the center of the microchannel is used for better visualization of the focusing and separation processes. (b) Time evolution of focusing and separation of the particles in the case of Wi = 1.3 and Re = 0.03. Due to the low Re, the inertia effect can be neglected and particles migrate due to the center- and wall-directed elastic lift forces. Blockage ratio is the key component for lateral migration of the particles in different equilibrium positions. After 4 s of oscillation (corresponding to an equivalent channel length of 76.4 mm), high-resolution separation can be achieved. (c) Cell lysate was introduced to the same microchannel as described in part (b) in a PEO$_{600kDa,0.5\%}$ solution, and similar behavior was observed. Larger organelles including cell nucleus are focused near the walls, while small organelles including GFP-fluorescently labeled p-bodies are focused at the centerline. Scale bars are 80 μm.

to 1 μm rigid particles, we demonstrate that p-bodies begin to focus at the center of the microchannel after 4 s of oscillation (Figure S1). In conclusion, we demonstrate for the first time efficient focusing of cellular organelles directly from a complex biological fluid using oscillatory viscoelastic focusing.

Throughput of Oscillatory Viscoelastic Microfluidic Platform. On first inspection, a potential weakness of the oscillatory platform stems from its low throughput, since the oscillation occurs within a single channel. However, this issue can be easily mitigated by fabricating an array of parallel microchannels to realize throughputs comparable to a continuous-flow focusing device. As shown in Figure S2b, a device incorporating 100 parallel channels (where w = 80 μm, h = 12 μm, and L = 4 mm) can be simply fabricated using photolithographic methods. Under continuous-flow operation (P = 2.5 bar), focusing of 1 μm particles is not possible due to the reduced length of the microchannel. Conversely, when operating under oscillatory flow conditions (oscillation frequency of 1 Hz) with the same flow condition (P = 2.5 bar), particles can be focused after only 4 s of oscillation, with a 2 orders of magnitude increase in analytical throughput when compared to oscillatory flow inside a single microchannel (increase of throughput from 50 counts/s to around 5000 counts/s). Indeed, as shown in Figure S2a, the parallel fluidic

circuit is analogous to an electric circuit, and thus an increase in the number of microchannels does not intensify the resistance of the whole system when using a pressure pump as a source.

Sample Recovery inside Oscillatory Viscoelastic Microfluidics. The recovery process incorporates two key steps. First, a mixture of unfocused (unseparated) particles oscillates until a "final" separation state is realized, and second, sample extraction at the outlets and new sample loading occur. To enable such an operation, we developed a software interface (oscillatory viscoelastic microfluidics, OVM, as shown in Figure S3a). This interface provides for control of the input parameters (oscillation frequency, number of oscillations, and sample loading time). The recovery process was demonstrated using a mixture of 1 and 3 μm particles. Initially, a mixture of these two populations is dispersed across the channel, with oscillations initiated by alternating the pressures applied to the inlet and the outlets (until a completely separated status is reached). Since particles enter the separation region with a precise alignment, they can be efficiently separated into two different outlets. Specifically, the larger 3 μm diameter particles can be sorted with a 98% efficiency (Figure S3b, Supplementary Movie S3) from outlet 1. The smaller 1 μm particles are collected from outlet 2 with a
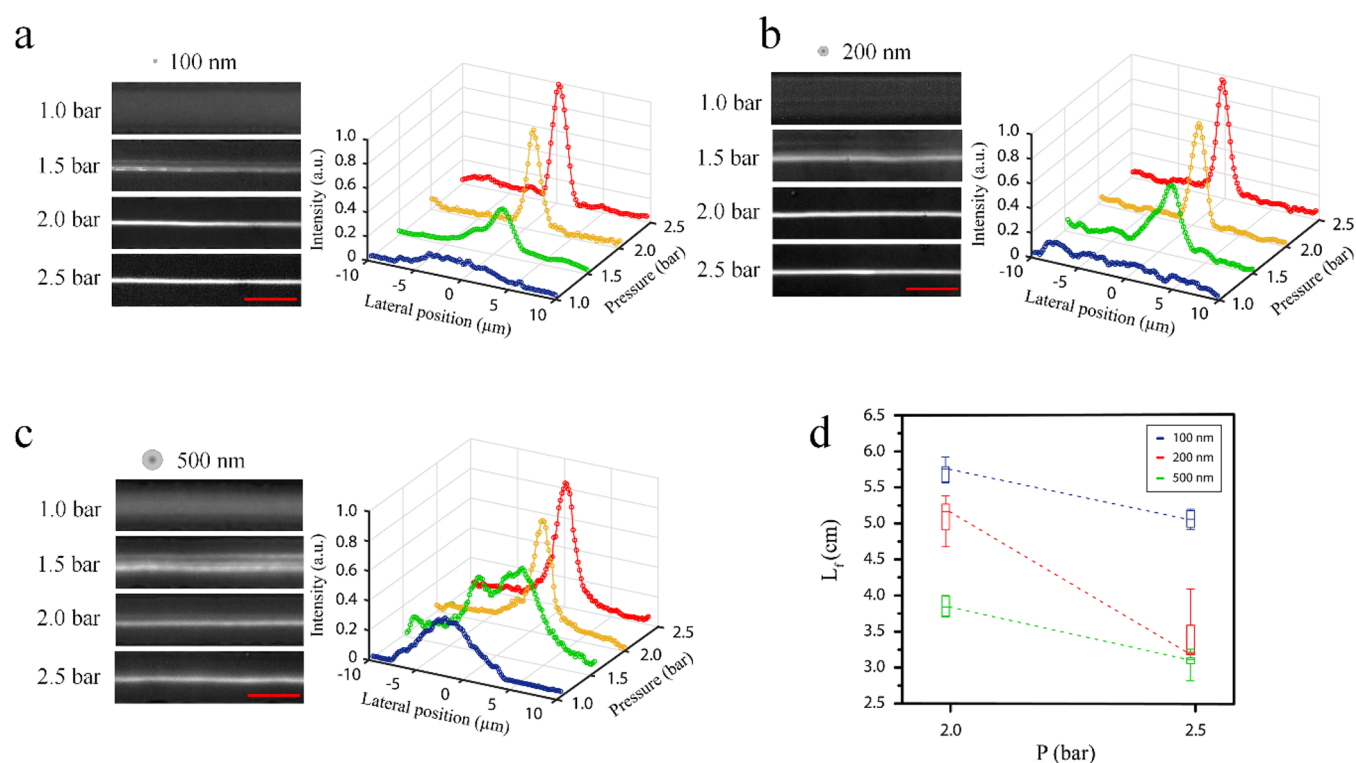
Figure 3. Effect of pressure on the focusing efficiency of 100, 200, and 500 nm particles within oscillatory viscoelastic microfluidics. The microchannel was fabricated using two-photon polymerization lithography with dimensions of 20 μm width, 1.4 μm height, and 4 mm length. (a, b, c) Effect of pressure (in terms of Wi and Re) on the focusing efficiency of nanoparticles in PEO$_{600kDa,1\%}$. In each case, images were recorded after 40 s of oscillation to ensure final focusing state. The Wi numbers for pressures at 1, 1.5, 2, and 2.5 bar are 0.26, 0.39, 0.52, and 0.65, respectively. The Re numbers for these pressures correspond to 0.00008, 0.00012, 0.00017, and 0.00021, respectively. Increasing the pressure results in dominant elastic forces enabling lateral migration of nanoparticles to minimum shear rate position. Since a high aspect ratio channel is used, most of the particles tend to migrate in the centerline. Blockage ratio values for 100, 200, and 500 nm in such a microchannel are 0.04, 0.08, and 0.2, respectively. (d) Diagram of focusing length vs pressure for 100 nm (β: 0.04), 200 nm (β: 0.08), and 500 nm (β: 0.2) nanoparticles. In the case of 2 bar (Wi: 0.52), L_f values for 100, 200, and 500 nm are 5.7, 5.1, and 3.8 cm, respectively. Increasing the pressure to 2.5 bar (Wi: 0.65) results in faster focusing of the particles with a similar trend, and L_f values for 100, 200, and 500 nm are 5.1, 3.4, and 3.1 cm, respectively. Scale bars are 20 μm.

separation efficiency of 100%. Subsequently, a new set of particles are loaded into the region of interest (the sorting region near the outlet) by application of continuous pressure to the inlet and zero pressure to the outlet.

Viscoelastic Nanoparticle Focusing Based on Oscillatory Flow. Next, we used the oscillatory viscoelastic microfluidic platform to focus nanoparticles, segmenting our study into two size regimes, namely, nanoparticles with dimensions equal to or larger than 100 nm (sub-micrometer regime) and nanoparticles with dimensions smaller than 100 nm (nanoregime). Initially, particles with diameters of 100, 200, and 500 nm were processed using an oscillation frequency of 2 Hz and pressures between 1 and 2.5 bar. The microfluidic device used for study of this size regime comprises a 4 mm long microchannel, having a height of 1.4 μm and a width of 20 μm. Figure 3 summarizes nanoparticle focusing behavior under the investigated conditions. At the highest pressure, Re is 0.0002, indicating that inertial effects are negligible (see Supplementary Note 3, Figure S4, Figure S5, and Figure S6). However, Wi values range from 0.26 (at 1 bar) to 0.65 (at 2.5 bar), which seems to be sufficiently high to induce lateral migration and focusing of nanoparticles. Indeed, for all particle diameters, we observed complete focusing at pressures of 2 and 2.5 bar, as shown by the fluorescence images obtained after 40 s (Figure 3a−c). Specifically, for 100, 200, and 500 nm

nanoparticles at a pressure of 2.5 bar, focusing efficiencies were 86%, 85%, and 90%, respectively. Accordingly, pressure values between 2 and 2.5 bar (0.52 < Wi < 0.65) allow for the efficient focusing of nanoparticles with diameters between 100 and 500 nm (and blockage ratios between 0.04 and 0.2) at the channel centerline.

It is important to note that it has been shown in high aspect ratio channels, plane focusing occurs.[31,61] However, our results demonstrate that by implementing oscillatory flow inside a viscoelastic medium, single-file focusing can be achieved even at high aspect ratio microchannels (for details, see Supplementary Note 4, Figure S7, and Figure S8).

We next estimated the focusing length, $L_f = Ut_f$, where t_f is the time required for particles to reach a stable minimum fwhm and U is the longitudinal velocity of particles traveling at the centerline. As illustrated in Figure 3d, this yielded focusing lengths at 2 bar ($Wi = 0.52$ and $Re = 0.000 17$) of 5.7 cm for 100 nm particles ($\beta = 0.04$), 5.1 cm for 200 nm particles ($\beta = 0.08$), and 3.8 cm for 500 nm particles ($\beta = 0.2$). At 2.5 bar ($Wi = 0.65$ and $Re = 0.000 21$), focusing lengths for 100, 200, and 500 nm particles decreased to 5.1, 3.4, and 3.1 cm, respectively, due to the higher exerted elastic forces. This analysis illustrates the fact that as the particle size is reduced, a longer channel is needed for centerline focusing and that an increase in pressure (or elasticity) accelerates the focusing
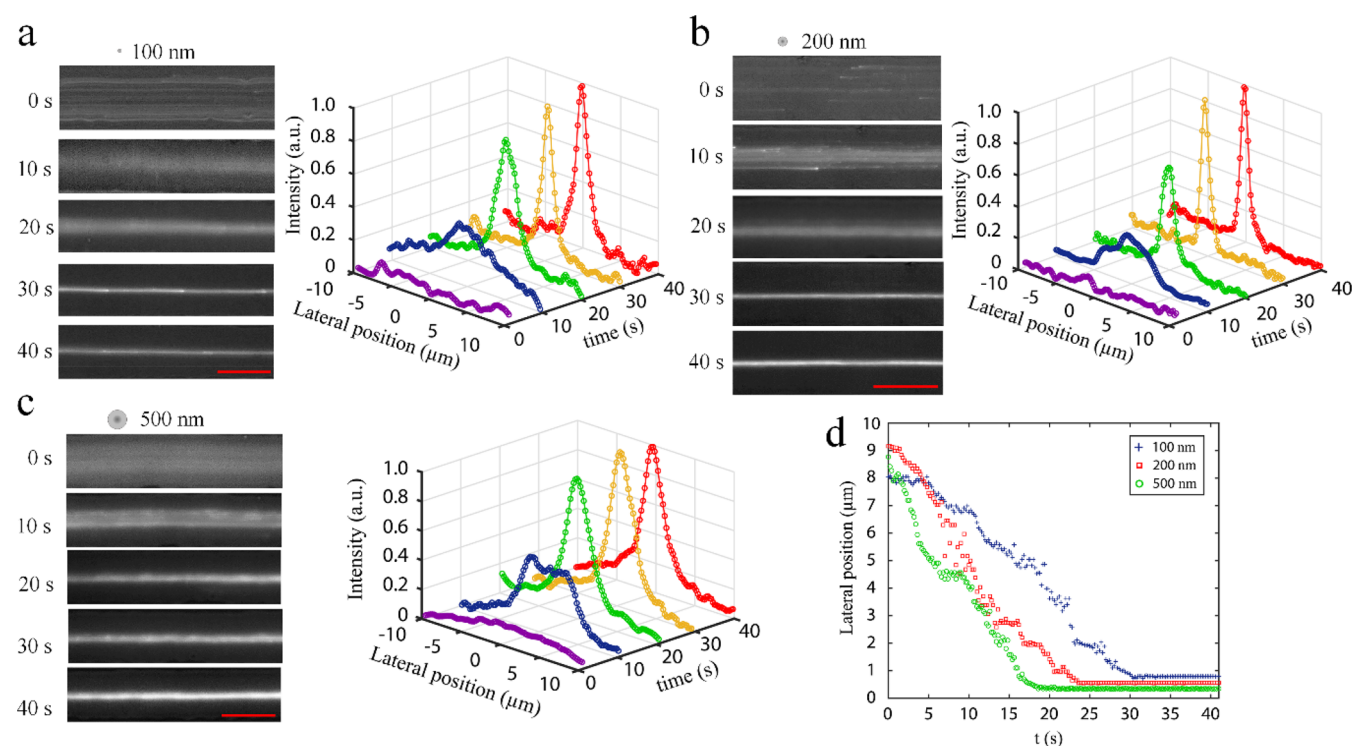
Figure 4. Time evolution of nanoparticles in oscillatory flow microfluidics *vs* focusing efficiency of (a) 100 nm, (b) 200 nm, and (c) 500 nm nanoparticles. (a) For 100 nm particles and a pressure of 2.5 bar (Wi = 0.65 and Re = 0.0002), a time period of 30 s is adequate to reach the final focusing state. Similarly, for 200 nm (b) and 500 nm particles (c), time periods of 30 and 20 s are needed for the final focusing state. (d) Single-nanoparticle tracking reveals similar behavior. In the case of 100, 200, and 500 nm, it takes approximately 18, 24, and 30 s for the individual particles to migrate from the wall (around 8 μm away from center to center) to the centerline. Scale bars are 20 μm.

process. Next, the time evolution of the focusing process was analyzed over a period of 40 s. For 100 and 200 nm particles, single-file focusing was accomplished in 30 s, while 500 nm particles were focused into a single-file configuration within 20 s (Figure 4a−c). Supplementary Movies S4 and S5 illustrate the time evolution and final focusing state of 500 nm particles. One of the most useful features of oscillatory viscoelastic microfluidic systems is the facility to perform single-particle tracking. As shown in Figure 4d, characteristic focusing times extracted from single-particle trajectories (from near the wall to the focusing position) were 30 s for 100 nm particles, 24 s for 200 nm particles, and 18 s for 500 nm particles. An additional advantage of oscillatory viscoelastic microfluidic systems is the ability to access high flow velocities (to improve focusing efficiency) through the use of short channel lengths. For instance, in the current study a 4 mm long channel was used for all experiments. For an analogous continuous-flow system incorporating the same microchannel cross-section, a length of approximately 4 cm (and a 10-fold increase in pressure) would be needed to attain an equivalent focusing efficiency.

To further investigate the effect of the blockage ratio on particle migration within the nanoregime, the platform was used to process 200, 500, and 1000 nm diameter nanoparticles flowing through high aspect ratio microchannels. Representative fluorescence images and corresponding intensity profiles at different blockage ratios are shown in Figure S9. As previously noted, for a microchannel with a height of 1.4 μm, both 200 nm (β: 0.076) and 500 nm (β: 0.19) nanoparticles were focused at the center of the microchannel (Figure S9; left). For the larger 1 μm particles, the blockage ratio is higher (β:

0.382), and thus they are aligned at off-center focusing positions regardless of their initial positions, while 500 nm (β: 0.19) particles are focused at the centerline (Figure S9; bottom). This behavior can be observed from the images recorded at the final equilibrium condition and the corresponding normalized fluorescence intensity (NFI) profiles for both 500 nm (one peak) and 1 μm (two-curve profile) particles. By decreasing the channel height to 700 nm and using a pressure of 4 bar (Wi = 0.53 and Re = 0.000 045), two off-center focusing positions are formed in the case of 500 nm particles (β: 0.137), while 200 nm nanoparticles (β: 0.148) are squeezed at the centerline (Figure S9; right). Accordingly, oscillatory viscoelastic microfluidics should allow for the efficient separation of nanometer-sized bioparticles, such as exosomes from large extracellular vesicles or cell-free DNA from plasma and platelets.

It is now recognized that the focusing, detection, and isolation of bioparticles with dimensions below 100 nm represent one of the most important challenges in the field of cell-free RNA diagnostics.[1] In this regard, the realization of a method able to robustly focus and isolate nanoparticles with hydrodynamic radii below 100 nm will potentially revolutionize our ability to isolate and process sEVs. Initial experiments aimed at focusing 20 and 40 nm diameter nanoparticles in microchannels having a width of 20 μm, a height of 1.4 μm, and a length of 4 mm failed to demonstrate efficient focusing performance. Accordingly, the channel height was reduced to 700 nm, while keeping all other dimensions constant. Using such a device, the effect of pressure on focusing efficiency was first evaluated, with images taken after 40 s of oscillation at a frequency of 2 Hz. As can been seen in
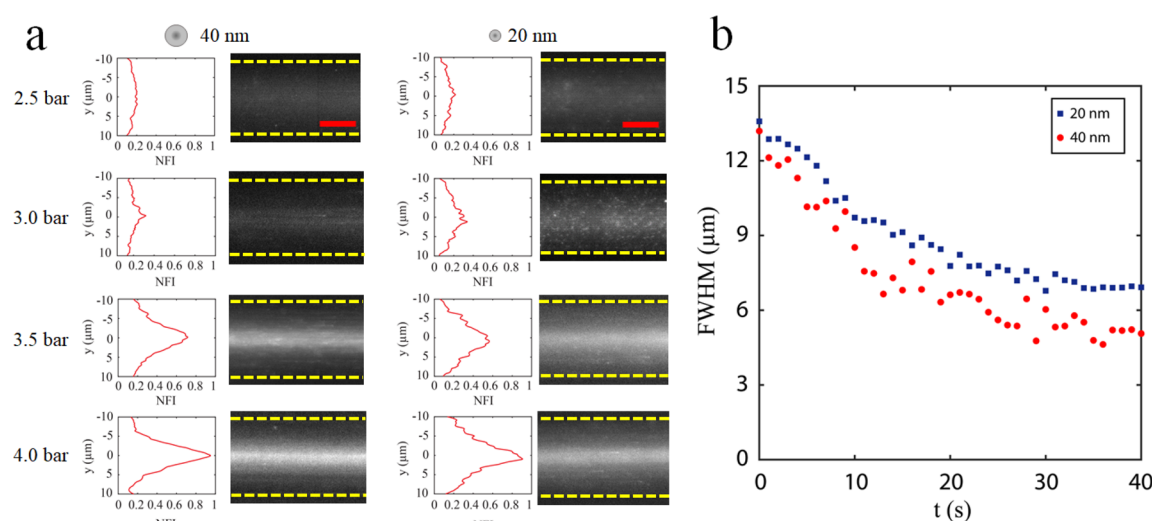
Figure 5. Focusing of 20 and 40 nm particles in oscillatory viscoelastic microfluidics. (a) Effect of pressure (in terms of *Wi* and *Re*) on the focusing efficiency of nanoparticles. For pressure values below 3.5 bar, no focusing was observed. Pressures of 3.5 (*Wi* = 0.47 and *Re* = 0.000 039) and 4 bar (*Wi* = 0.53 and *Re* = 0.000 045) resulted in focusing of the nanoparticles at the center of the channel. Images for each case were recorded after 40 s of oscillation at a frequency of 2 Hz. (b) fwhm values were calculated at a pressure of 4 bar. fwhm values reached a final value of 4.95 and 6.95 μm for 40 and 20 nm, respectively. Scale bars are 10 μm.
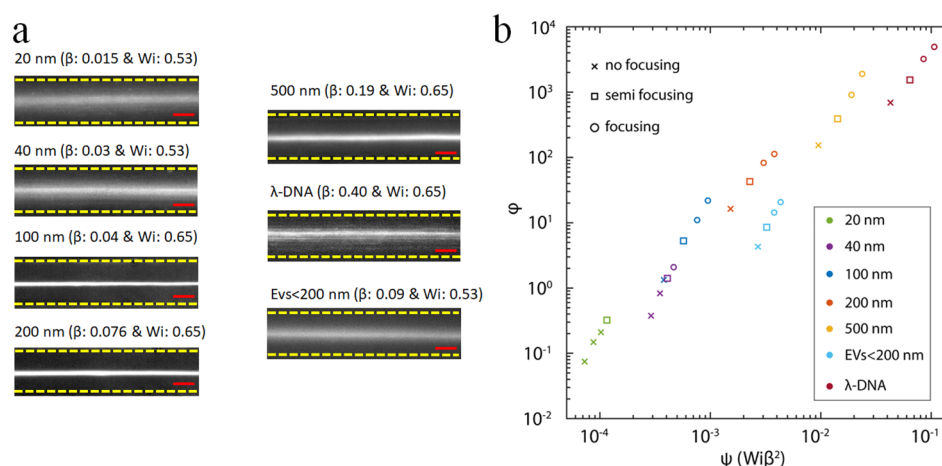

Figure 6. Experimental analysis of focusing phase explored in this study. (a) Final focusing states at specific blockage ratios and *Wi* numbers for 20, 40, 100, 200, and 500 nm particles, λ-DNA molecules, and EVs (less than 200 nm). Scale bars are 10 μm. (b) Dimensionless diffusion number (φ) versus dimensionless elastic force number (ψ) for different focusing patterns (focusing, semifocusing, and no focusing).

Figure 5a, 40 nm particles begin to align at the center of the channel at a pressure of 3.5 bar (*Wi* = 0.47, *Re* = 0.000 039, β = 0.03), with a further increase in pressure to 4 bar (*Wi* = 0.53, *Re* = 0.000 045, β = 0.03) resulting in an improved focusing efficiency of 61% (Supplementary Movie S6). Similar behavior is observed in the case of 20 nm diameter nanoparticles (β = 0.015), with a focusing efficiency of 51% being achieved at 4 bar (*Wi* = 0.53). As shown in Figure 5b, fwhm values of 4.95 and 6.95 μm were realized after an oscillation period of 40 s, for 40 and 20 nm particles, respectively.

Viscoelastic Bionanoparticle Focusing Based on Oscillatory Flow. On the basis of such excellent focusing performance, we used the oscillatory viscoelastic microfluidic platform to focus λ-DNA and a population of mNG-labeled sEVs concentrated from cell culture conditioned medium. λ-DNA molecules have a radius of gyration of 530 nm, but are more challenging to focus at the channel centerline than rigid particles of a similar size. Experiments involving λ-DNA were performed using the sub-micrometer regime microfluidic

device (comprising a channel that is 20 μm wide, 1.4 μm high, and 4 mm long). As can be seen in Figure S10a, λ-DNA molecules were focused at the channel centerline (after 30 s). Under these conditions, *Wi* > 0.52 induces sufficient elastic force to focus λ-DNA molecules. Indeed, when *Wi* = 0.65 and *Re* = 0.0002, the focusing efficiency reaches 71.5%. Experiments involving sEVs (with a mean diameter of 122 nm; Figure S11) were performed using the nanoregime microfluidic device (Figure S10b). Using an oscillation frequency of 2 Hz and a pressure of 4 bar, a focusing time of 25 s and focusing efficiency of 67.4% were realized. These data confirm that biological species with dimensions ranging from a few micrometers to a hundred nanometers can be precisely manipulated and focused at specific regions of a microchannel through the combination of viscoelastic forces and oscillatory flows.

It is well known that differences in size, density, and surface marker properties of EV populations are associated with distinct RNA/protein signatures[59] that can be exploited in

diagnostic assays. To showcase the possibility that our oscillatory viscoelastic microfluidic platform can be used for the efficient separation and focusing of biologically relevant particles, we demonstrated the separation of two populations of EVs that differ in size: mNeonGreen-labeled small EVs (sEVs) produced by *in vitro* cultured cells and EVs (milk fat globules, MFG) from bovine milk labeled with MemBright (a red-fluorescent membrane dye). MFGs are low-density and large extracellular vesicles produced by lactocytes and represent the main carrier of triglyceride in milk. We assessed the focusing and separation of these EVs both in individual and in a mixture run. As can be seen in Figure S12, for both individual and mixture experiments, sEVs (100 nm) are focused at the centerline, while MFGs (1−2 μm) are focused near the channel walls at Re = 0.001 and Wi = 1.5. The microfluidic device used for this study comprises a 4 mm long microchannel, with a height of 2 μm and a width of 20 μm.

Viscoelastic Focusing on a Diffusion−Elasticity State Space Map. The operating flow regimes associated with nanoparticle size and viscoelastic focusing can be depicted using a diffusion−elasticity state space map (Figure 6). Since the Reynolds number is negligible and inertial effects are insufficient for lateral migration of particles, the two main forces responsible for the transverse migration of particles are the elastic force due to fluid elasticity and the Brownian force due to diffusion. These two forces can be compared using the dimensionless number φ, which is defined as the ratio of lateral velocity (u_p) due to elastic effect to the diffusion constant of the particle (D) within the viscoelastic carrier fluid within a given length L_c, i.e.,

$$\varphi = L_c \frac{u_p}{D} \tag{1}$$

Ho and Leal[28] and Brunn[29,60] have developed a theoretical approach to model particle motion in a second-order fluid. By using the force equation from these models, assuming a negligible second normal stress difference ($N_2 \approx 0$), and considering only the first normal stress difference $N_1 = 2\eta\tau\dot{\gamma}^2$, the elastic lift force on a particle can be approximated as

$$F_{el} = -A\eta u_x r_p Wi\beta^2 z^* \tag{2}$$

where A is a prefactor, η the viscosity, u_x the mean longitudinal velocity, r_p the radius of the particle, Wi the Weissenberg number, β the blockage ratio, and $z^* = z/H$ the dimensionless lateral position factor.[61] By balancing the elastic and drag forces ($F_{drag} = 6\pi\eta r_p u_p$) and for a non-Brownian case, we can extract the lateral velocity of the particle, i.e.,

$$u_p = \frac{A}{6\pi} u_x Wi\beta^2 z^* \tag{3}$$

To properly describe the diffusivity of the nanoparticles in a viscoelastic fluid, short time effects (fast diffusion; see Supplementary Note 5) are neglected and the generalized Stokes−Einstein relation is adopted as follows:[51,62]

$$D = \frac{K_b T}{3\pi\eta(a + 2\delta)} \tag{4}$$

where K_b is the Boltzmann constant, T the absolute temperature, a the diameter of the particle, δ the thickness of the depletion layer created around the nanoparticle (see Supplementary Note 5) within the viscoelastic fluid, and η the macroscopic viscosity of the polymer solution. By replacing eq

3 and eq 4 in eq 1 and considering the characteristic length (L_c) as the hydraulic diameter of the microchannel (D_h), we get

$$\varphi = \frac{A\eta D_h}{4 K_b T} u_x(a + 2\delta)Wi\beta^2 z^* \tag{5}$$

This dimensionless number (φ) provides a measure of the relative magnitudes of the elastic and Brownian forces. A is a prefactor and, according to studies by Ho and Leal, is equal to 5π, while Brunn reports a value of $22\pi/5$.[28,60] Herein, the values of A and z^* are chosen to be 5π and 1, respectively, to allow comparison of φ values for different particle sizes, channel dimensions, flow conditions, and elasticity.

The lateral migration velocity in a viscoelastic fluid scales as $\psi = Wi\beta^2$.[28,60] Accordingly, eq 5 can be written as

$$\varphi = \frac{5\pi\eta D_h}{4 K_b T} u_x(a + 2\delta)\psi \tag{6}$$

Hence, φ values were calculated for Brownian particles (i.e., 20, 40, 100, 200, 500 nm nanoparticles), EVs less than 200 nm in diameter, and λ-DNA molecules, and a diffusion−elasticity state space map was constructed (Figure 6b). For 20 and 40 nm particles, the magnitudes of elasticity and Brownian motion are similar and diffusion is not negligible. However, an increase in Wi leads to a better focusing state, as shown in Figure 6b. Interestingly, for the case of 40 nm particles we noticed that an increase in pressure initially leads to a transition between a nonfocusing state and a semifocusing state and then a transition to focusing state (when $\varphi \approx 2$). For 20 nm particles, the focusing condition was improved to a semi-focusing state for the flow condition explored in this study ($\varphi \approx 0.3$). For the remaining nanoparticles, φ values are much higher than 1 even at low flow rates, suggesting efficient suppression of Brownian motion for particles in the sub-micrometer regime. Accordingly, particle focusing can simply be improved by increasing the pressure (or Wi). This leads to a considerable elastic force that induces lateral migration of particles along the centerline of the channel and (for 40, 100, 200, 500 nm, EVs, and λ-DNA particles) a transition from a nonfocusing state to a semifocusing state and finally to a single-file focusing state. Such a simplified dimensional analysis of diffusion and elasticity for flow conditions, rheological properties, and channel geometry is highly useful. However, in more complicated cases (e.g., elasto-inertial regimes or flow within curved conduits), this model should be generalized.

CONCLUSION

In this study, we have demonstrated the utility of oscillatory viscoelastic microfluidic systems for manipulating and focusing objects that range in size from 20 nm up to a few micrometers. This study addresses three key size regimes, namely, the micrometer, sub-micrometer, and nanoregimes. Results show that 1, 5, and 10 μm particles could be efficiently focused at distinct parts of a (microregime) microchannel through control of the blockage ratio. When cell lysate was introduced to the same platform, we achieved focusing of cellular organelles (p-bodies) with a similar efficiency to that observed for rigid particles. Within the sub-micrometer regime, 100, 200, and 500 nm diameter nanoparticles and λ-DNA molecules were successfully focused at the center of a microchannel using oscillatory viscoelastic microfluidics. Critically, and through simple modification of channel dimensions, this method could

also be used for the effective separation of nanoparticles. Finally, within the nanoregime, 20 and 40 nm diameter particles and sEVs (smaller than 200 nm in size) were also focused in a rapid and robust manner. To conclude, a dimensionless parameter (φ) was introduced to compare Brownian with elastic forces and used to show that the combination of a viscoelastic fluid and oscillatory flow suppresses Brownian motion. The presented oscillatory viscoelastic microfluidic methodology enables particle manipulation over a wide size range and has significant immediate utility in the rapid isolation of EVs, cell-free DNA, viruses, protein aggregates, λ-DNA, cellular organelles (RNA granules), and various types of cells.

MATERIALS AND METHODS

Device Design and Fabrication. Two methods were used in the fabrication of microfluidic master molds. First, conventional lithographic techniques were used to create fluidic structures with micrometer-scale dimensions. Briefly, microchannel patterns were designed using AutoCAD 2018 (Autodesk, San Rafael, CA, USA) and printed onto a 177 μm thick fine grain emulsion film (Micro Lithography Services Ltd., Chelmsford, UK) to form a photomask. This photomask was then utilized to pattern an SU-8 coated silicon wafer (Microchem Corporation, Westborough, MA, USA). The final master structure consisted of an inverted straight rectangular microchannel (width 80 μm, height 12 μm) with a total length of 4 mm and an expansion channel (width 400 μm, height 12 μm) to facilitate the visualization process during image acquisition. Smaller fluidic features were created using a Photonic Professional GT2 two-photon polymerization 3D printer (Nanoscribe GmbH, Stutensee, Germany). Specifically, the printer was used to directly form microfluidic structures on indium tin oxide-coated glass using a 63× objective and an IP-Dip photoresist (Nanoscribe GmbH). After the printing was completed, the mold was developed in poly(ethylene glycol) methacrylate (Sigma, Buchs, Switzerland) for 15 min and cleaned in isopropanol for a further 5 min. The final master structure consists of an inverted 4 mm long microchannel, having a height of 1.4 μm and a width of 20 μm. The smallest master mold consisted of an inverted 4 mm long microchannel, having a height of 700 nm and a width of 20 μm.

Subsequently, a 10:1 mixture of polydimethylsiloxane (PDMS) monomer and curing agent (Sylgard 184, Dow Corning, Midland, MI, USA) was poured over the master mold and peeled off after polymerization at 70 °C for 4 h. Inlet and outlet ports were created using a hole-puncher (Technical Innovations, West Palm Beach, FL, USA). Afterward, the structured PDMS substrate was bonded to a glass substrate (Menzel-Glaser, Monheim am Rhein, Germany) after treating both surfaces in an oxygen plasma (EMITECH K1000X, Quorum Technologies, UK) for 60 s. PDMS devices used for the micrometer and sub-micrometer regime experiments were bonded to a 1 mm thick glass, while a 200 μm thick glass substrate was used for nanoregime experiments.

Flow Control Instrumentation. A home-built system was used to generate and control oscillatory flows within microfluidic devices (Figure 1a). The system comprised an UNO REV3 Arduino board (Distrelec, Uster, Switzerland), a homemade digital-to-analog conversion circuit board, solenoid valves (FESTO, Esslingen, Germany), and a GUI control interface developed in Microsoft Visual Studio using C++. Commands from the GUI interface are sent to the Arduino board and used to control the solenoid valves at frequencies up to 20 Hz.

Viscoelastic Fluid Preparation and Characterization. Viscoelastic fluids were prepared by completely dissolving poly(ethylene oxide) (PEO, M_w = 600 kDa; Sigma-Aldrich, Switzerland) in deionized water to a concentration of 1% (w/v). Solutions produced in this manner were then aged at 4 °C for 1 week to realize a steady-state viscosity. Viscosities of all fluids (Figure S13a) were measured at room temperature using a rheometer (MCR 502, Anton Paar,

Germany) and a double gap cylinder (DG 26.7). Deionized water exhibited a constant viscosity of 0.89 cP. The viscosity of $PEO_{600kDa,1\%}$ was measured to be between 33.2 and 10.3 cP, exhibiting shear-thinning behavior. Additionally, the viscosity of $PEO_{600kDa,4\%}$ was measured to be between 846.3 and 110.1 cP, showing stronger shear-thinning behavior. Finally, the shear stress−strain curve was measured and used to uncover concentration-dependent hysteresis effects. Figure S13b shows the shear stress−strain dependence for both of the $PEO_{600kDa,1\%}$ and $PEO_{600kDa,4\%}$ samples. It can be seen that hysteresis is significantly smaller for the $PEO_{600kDa,1\%}$ sample. High hysteresis can result in asymmetric and unpredictable lateral motion of the particles during oscillation. Considering both low hysteresis and low shear-thinning for $PEO_{600kDa,1\%}$, we chose $PEO_{600kDa,1\%}$ as the viscoelastic carrier fluid. We also performed COMSOL numerical simulations with a view to predicting the shear rates involved in the oscillatory flow device (for the flow conditions used in experiment, micrometer regime: Re = 0.03, Wi = 1.3, sub-micrometer regime: Re = 0.00021, Wi = 0.65, and nanoregime: Re = 0.000045, Wi = 0.53). Figure S14 depicts the shear rate distribution within the cross-section for each case. The shear rate varies between 717 and 7118 s^{-1} in the micrometer regime, between 566 and 3186 s^{-1} in the sub-micrometer regime, and between 507 and 3189 s^{-1} in the nanoregime. For the Reynolds number calculation, we used a viscosity value of 10.3 cP since the PEO solution exhibits constant viscosity behavior (see Figure S13) in all shear rate ranges.

Working Principle and Data Acquisition. Samples were loaded into glass vials (ThermoFisher Scientific, Waltham, MA, USA) and delivered to the microfluidic device at a given pressure using an air pressure source. The microfluidic device was mounted on an inverted Eclipse Ti-E microscope (Nikon, Zürich, Switzerland) equipped with an IDT high-speed camera (Motion Pro Y5.1, Niederoenz, Switzerland) and an ORCA-flash 4.0 CMOS camera (Hamamatsu, Solothurn, Switzerland). Bright-field imaging of particle populations and cell lysate was carried out using the high-speed camera, plasma light source illumination (HPLS200 series Thorlabs, Newton, NJ, USA), and a 20×, 0.45 NA S Plan Fluor objective (Nikon, Switzerland). Fluorescence imaging was performed using two different objectives. For the visualization of 100, 200, and 500 nm particles, p-bodies, and λ-DNA, a 20×, 0.45 NA objective lens was used. In addition, a 60×, 1.2 NA WI Plan Apo VC objective (Nikon, Switzerland) was used to image 20 and 40 nm particles and extracellular vesicles. Images were processed with ImageJ software (U.S. National Institutes of Health, Bethesda, MD, USA) using the "z-projection" and "sum slices" options. To assess focusing performance, full width at half-maximum (fwhm) values were extracted from intensity profiles, with focusing efficiency being defined as the fraction of species within 1/4 microchannel width from the centerline. For bright-field experiments, the probability distribution function (PDF) was obtained by measuring the fraction of the particles in the expansion region.

Sample Preparation. Polystyrene (PS) beads with an average diameter of 10, 5, and 1 μm (Sigma-Aldrich, Switzerland) as well as fluorescent particles with average diameters of 500, 200, 100, 40, and 20 nm (Invitrogen, Carlsbad, CA, USA) were dispersed in deionized water at a concentration of 10^6 particles/mL. For fluorescence labeling of λ-DNA (Sigma-Aldrich, Switzerland), 0.2 μM YOYO-1 (ThermoFisher Scientific, USA) was dissolved in an aqueous solution containing 60 μM Netropsin (Sigma-Aldrich, Switzerland), 10 μM TBE buffer (Medicago, Uppsala, Sweden), and 2-mercaptoethanol (Sigma-Aldrich, Switzerland). This was subsequently added to the PEO_{600kDa} solution to a final concentration of 0.5% (w/v).

Cell Lines. HEK293T flp-in TREX cells (Life Technologies, Zug, Switzerland) were maintained at 37 °C within a (5% CO_2) Dulbecco's modified Eagle medium (Life Technologies, Switzerland) containing 4500 g/mL glucose and further supplemented with 10% fetal bovine serum (FBS) (Life Technologies, Switzerland), 100 U/mL of penicillin (Sigma-Aldrich, Switzerland), and 100 μg/mL of streptomycin (Sigma-Aldrich, Switzerland).

Cell Lysis for p-Body Purification. First, 8×10^7 HEK293T Flp-in TREX cells, stably expressing the mNeonGreen (mNG)-tagged

Ago2 transgene, were seeded in 15 cm dishes with 2 μg/mL doxycycline (DOX) (Sigma-Aldrich, Switzerland) being used to induce protein expression. Two days after seeding, approximately 3×10^7 million cells were trypsinized and washed twice with PBS buffer before snap freezing the cell pellet and subsequent storage at −80 °C. Before delivery to the microfluidic device, frozen cell pellets were homogenized and lysed for 20 min on a rotating wheel at 4 °C using the following lysis buffer: 0.15 M NaCl (Carl Roth, Arlesheimm, Switzerland), 50 mM Tris pH = 7.5 (Carl Roth, Switzerland), 15 mM MgCl$_2$ (Carl Roth, Switzerland), 200 μM phenylmethylsulfonyl fluoride (Sigma-Aldrich, Switzerland), 5% glycerol (Brunschwig, Basel, Switzerland), and 0.2% Triton-X (Carl Roth, Switzerland), supplemented by one tablet of Complete Mini EDTA-free protease inhibitor cocktail (Sigma-Aldrich, Switzerland) per 7 mL of lysis buffer.

EV Purification. For EV purification experiments, HEK293T cells expressing mNG-HRAS (FSN-HRAS) or mNG-KRAS (FSN-KRAS) were conditioned to grow in Pro293a-chemically defined medium (CDM; Lonza, Visp, Switzerland) supplemented with 1% FBS medium, by reducing the FBS content by splitting (starting from 10%). Conditioned cells were split with Accutase (STEMCELL Technologies, Köln, Germany) instead of Trypsin. Pro293a-CDM was always supplemented with 100 U/mL of penicillin and 100 μg/mL of streptomycin.

To prepare conditioned culture medium (CCM) containing fluorescent microvesicles, 20×10^7 HEK293T FT FSN-HRAS and FSN-KRAS cells (grown in 1% FBS Pro293a-CDM) were seeded in 15 cm dishes with Pro293a-CDM without FBS. The next day protein expression was induced by addition of 2 μg/mL DOX to the medium. After 3 days of cell growth, CCM from two 15 cm plates was collected in one 50 mL Falcon tube. To remove residual cells, CCM was spun for 5 min at 500g. Supernatant was then transferred to a fresh tube, and samples were spun for an additional 5 min at 1000g. Supernatant was serially filtered using syringe filters with cut-offs of 0.8 and 0.2 μm, before concentrating the CCM down to 500 μL using a Centricon 70 Plus centrifugal filter (Sigma-Aldrich, Switzerland) according to the manufacturer's protocol (concentration step: 35 min at 2200g at 18 °C; collection step: 2 min at 1000g at 18 °C).

Milk Fat Globule Purification. MFGs were isolated from fresh bovine milk (Milchautomat, Hönggerberg, Switzerland). In brief, 50 mL of milk was spun at 500g for 5 min in a Falcon tube. Subsequently, the top layer containing large MGFs (>3 μm) was discarded, and the milk then spun at 2000g for an additional 5 min. The top layer (enriched in small MFGs) was collected and resuspended in 50 mL of PBS, spun at 2000g for 5 min, and then collected in the top layer before final resuspension in 1−2 mL of PBS. Red-fluorescent MFGs were prepared by mixing 300 μL of an 800 nM solution of Lipilight 590 nm (MemBright. Idylle, France) in PBS, with 300 μL of PBS-washed MFGs, and incubating for 30 min in the dark. Labeled MFGs were spun at 2000g for 5 min, with the top layer being collected and resuspended in 600 μL of PBS before use.

ASSOCIATED CONTENT

Ⓢ Supporting Information

The Supporting Information is available free of charge at https://pubs.acs.org/doi/10.1021/acsnano.9b06123.

Additional information, figures, and tables (PDF)

Movie S1: Time evolution of oscillatory focusing and separation of 1, 5, and 10 μm particles (AVI)

Movie S2: Final focusing and separation state of 1, 5, and 10 μm particles (AVI)

Movie S3: Sample recovery inside oscillatory viscoelastic microfluidics (AVI)

Movie S4: Time evolution of oscillatory focusing of 500 nm particles (AVI)

Movie S5: Final focusing state of 500 nm particles (AVI)

Movie S6: Final focusing state of 40 nm particles (AVI)

AUTHOR INFORMATION

Corresponding Authors

*E-mail: stavros.stavrakis@chem.ethz.ch.
*E-mail: andrew.demello@chem.ethz.ch.

ORCID ⓘ

Xiaobao Cao: 0000-0003-2211-2823
Stavros Stavrakis: 0000-0002-0888-5953
Andrew J. deMello: 0000-0003-1943-1356

Author Contributions

M.A., S.S., and A.d.M. conceived the project and devised the research plan. M.A., X.C., and M.K.A. developed the instrumental platform and methodology. M.A. performed all experiments. X.C. fabricated all microfluidic devices. B.M. and D.V.L. developed the protocols for cell culturing and extracellular vesicle purification. M.A., S.S., B.M., and A.d.M. wrote the manuscript.

Notes

The authors declare no competing financial interest.
A preliminary version of this work is available in BioRxiv.[63]

REFERENCES

(1) Mateescu, B.; Kowal, E. J. K.; van Balkom, B. W. M.; Bartel, S.; Bhattacharyya, S. N.; Buzás, E. I.; Buck, A. H.; de Candia, P.; Chow, F. W. N.; Das, S.; Driedonks, T. A. P.; Fernández-Messina, L.; Haderk, F.; Hill, A. F.; Jones, J. C.; Van Keuren-Jensen, K. R.; Lai, C. P.; Lässer, C.; di Liegro, I.; Lunavat, T. R.; Lorenowicz, M. J.; Maas, S. L. N.; et al. Obstacles and Opportunities in the Functional Analysis of Extracellular Vesicle RNA - An ISEV Position Paper. *J. Extracell. Vesicles* **2017**, *6*, 1286095.

(2) Schwab, A.; Meyering, S. S.; Lepene, B.; Iordanskiy, S.; van Hoek, M. L.; Hakami, R. M.; Kashanchi, F. Extracellular Vesicles from Infected Cells: Potential for Direct Pathogenesis. *Front. Microbiol.* **2015**, *6*, 1132.

(3) Jansen, F.; Nickenig, G.; Werner, N. Extracellular Vesicles in Cardiovascular Disease. *Circ. Res.* **2017**, *120*, 1649−1657.

(4) D'Souza-Schorey, C.; Clancy, J. W. Tumor-Derived Microvesicles: Shedding Light on Novel Microenvironment Modulators and Prospective Cancer Biomarkers. *Genes Dev.* **2012**, *26*, 1287−1299.

(5) Schwarzenbach, H.; Hoon, D. S. B.; Pantel, K. Cell-Free Nucleic Acids as Biomarkers in Cancer Patients. *Nat. Rev. Cancer* **2011**, *11*, 426−437.

(6) Théry, C.; Amigorena, S.; Raposo, G.; Clayton, A. Isolation and Characterization of Exosomes from Cell Culture Supernatants and Biological Fluids. *Curr. Protoc. Cell Biol.* **2006**, *30*, 3−22.

(7) Livshits, M. A.; Khomyakova, E.; Evtushenko, E. G.; Lazarev, V. N.; Kulemin, N. A.; Semina, S. E.; Generozov, E. V.; Govorun, V. M. Isolation of Exosomes by Differential Centrifugation: Theoretical Analysis of a Commonly Used Protocol. *Sci. Rep.* **2015**, *5*, 17319.

(8) Scott, A. M.; Tauro, B. J.; Ji, H.; Mathias, R. A.; Greening, D. W.; Simpson, R. J.; Mathivanan, S. Comparison of Ultracentrifugation, Density Gradient Separation, and Immunoaffinity Capture Methods for Isolating Human Colon Cancer Cell Line LIM1863-Derived Exosomes. *Methods* **2012**, *56*, 293−304.

(9) Lari, E.; Fondelli, C.; Gavrilova, J.; Corrado, A.; Zocco, D.; Radano, G.; Chiesi, A.; Muhhina, J.; Zarovni, N.; Guazzi, P. Integrated Isolation and Quantitative Analysis of Exosome Shuttled Proteins and Nucleic Acids Using Immunocapture Approaches. *Methods* **2015**, *87*, 46−58.

(10) Sturk, A.; Nieuwland, R.; Coumans, F. A. W.; Böing, A. N.; van der Pol, E.; Grootemaat, A. E. Single-Step Isolation of Extracellular Vesicles by Size-Exclusion Chromatography. *J. Extracell. Vesicles* **2014**, *3*, 23430.

(11) Nordin, J. Z.; Lee, Yi.; Vader, P.; Mäger, I.; Johansson, H. J.; Heusermann, W.; Wiklander, O. P. B.; Hällbrink, M.; Seow, Y.; Bultema, J. J.; Gilthorpe, J.; Davies, T.; Fairchild, P. J.; Gabrielsson, S.; Meisner-Kober, N. C.; Lehtiö, J.; Smith, C. I. E.; Wood, M. J. A.; El Andaloussi, S. Ultrafiltration with Size-Exclusion Liquid Chromatography for High Yield Isolation of Extracellular Vesicles Preserving Intact Biophysical and Functional Properties. *Nanomedicine* **2015**, *11*, 879−883.

(12) Shurtleff, M. J.; Temoche-Diaz, M. M.; Karfilis, K. V.; Ri, S.; Schekman, R. Y-Box Protein 1 Is Required to Sort MicroRNAs into Exosomes in Cells and in a Cell-Free Reaction. *eLife* **2016**, *5*, 1−23.

(13) Kormelink, T. G.; Arkesteijn, G. J. A.; Nauwelaers, F. A.; van den Engh, G.; Nolte-'t Hoen, E. N. M.; Wauben, M. H. M. Prerequisites for the Analysis and Sorting of Extracellular Vesicle Subpopulations by High-Resolution Flow Cytometry. *Cytometry, Part A* **2016**, *89*, 135−147.

(14) Turk, J. R.; Guerrero, A.; Condello, D.; Narayanan, P. K.; Nolan, J. P.; Stoner, S. A.; Duggan, E. High Sensitivity Flow Cytometry of Membrane Vesicles. *Cytometry, Part A* **2016**, *89*, 196−206.

(15) Morales-Kastresana, A.; Telford, B.; Musich, T. A.; McKinnon, K.; Clayborne, C.; Braig, Z.; Rosner, A.; Demberg, T.; Watson, D. C.; Karpova, T. S.; Freeman, G. J.; DeKruyff, R. H.; Pavlakis, G. N.; Terabe, M.; Robert-Guroff, M.; Berzofsky, J. A.; Jones, J. C. Labeling Extracellular Vesicles for Nanoscale Flow Cytometry. *Sci. Rep.* **2017**, *7*, 1−10.

(16) Çetin, B.; Li, D. Dielectrophoresis in Microfluidics Technology. *Electrophoresis* **2011**, *32*, 2410−2427.

(17) Li, M.; Li, W. H.; Zhang, J.; Alici, G.; Wen, W. A Review of Microfabrication Techniques and Dielectrophoretic Microdevices for Particle Manipulation and Separation. *J. Phys. D: Appl. Phys.* **2014**, *47*, 063001.

(18) Hejazian, M.; Li, W.; Nguyen, N. T. Lab on a Chip for Continuous-Flow Magnetic Cell Separation. *Lab Chip* **2015**, *15*, 959−970.

(19) Laurell, T.; Petersson, F.; Nilsson, A. Chip Integrated Strategies for Acoustic Separation and Manipulation of Cells and Particles. *Chem. Soc. Rev.* **2007**, *36*, 492−506.

(20) Lin, S. C. S.; Mao, X.; Huang, T. J. Surface Acoustic Wave (SAW) Acoustophoresis: Now and Beyond. *Lab Chip* **2012**, *12*, 2766−2770.

(21) Yamada, M.; Nakashima, M.; Seki, M. Pinched Flow Fractionation: Continuous Size Separation of Particles Utilizing a Laminar Flow Profile in a Pinched Microchannel. *Anal. Chem.* **2004**, *76*, 5465−5471.

(22) McGrath, J.; Jimenez, M.; Bridle, H. Deterministic Lateral Displacement for Particle Separation: A Review. *Lab Chip* **2014**, *14*, 4139−4158.

(23) Cox, E. C.; Sturm, J. C.; Huang, L. R.; Austin, R. H. Continuous Particle Separation Through Deterministic Lateral Displacement. *Science* **2004**, *304*, 987−990.

(24) Di Carlo, D. Inertial Microfluidics. *Lab Chip* **2009**, *9*, 3038−3046.

(25) Asghari, M.; Serhatlioglu, M.; Saritas, R.; Guler, M. T.; Elbuken, C. Tape'n Roll Inertial Microfluidics. *Sens. Actuators, A* **2019**, *299*, 111630.

(26) Ozkumur, E.; Shah, A. M.; Ciciliano, J. C.; Emmink, B. L.; Miyamoto, D. T.; Brachtel, E.; Yu, M.; Chen, P.; Morgan, B.; Trautwein, J.; Kimura, A.; Sengupta, S.; Stott, S. L.; Karabacak, N. M.; Barber, T. A.; Walsh, J. R.; Smith, K.; Spuhler, P. S.; Sullivan, J. P.; Lee, R. J.; et al. Inertial Focusing for Tumor Antigen-Dependent and -Independent Sorting of Rare Circulating Tumor Cells. *Sci. Transl. Med.* **2013**, *5*, 179ra47−179ra47.

(27) Karnis, A.; Mason, S. G. Particle Motions in Sheared Suspensions. XIX. Viscoelastic Media. *Trans. Soc. Rheol.* **1966**, *10*, 571−592.

(28) Ho, B. P.; Leal, L. G. Migration of Rigid Spheres in a Two-Dimensional Unidirectional Shear Flow of a Second-Order Fluid. *J. Fluid Mech.* **1976**, *76*, 783−799.

(29) Brunn, P. The Motion of Rigid Particles in Viscoelastic. *J. Non-Newtonian Fluid Mech.* **1980**, *7*, 271−288.

(30) D'Avino, G.; Romeo, G.; Villone, M. M.; Greco, F.; Netti, P. A.; Maffettone, P. L. Single Line Particle Focusing Induced by Viscoelasticity of the Suspending Liquid: Theory, Experiments and Simulations to Design a Micropipe Flow-Focuser. *Lab Chip* **2012**, *12*, 1638−1645.

(31) Leshansky, A. M.; Bransky, A.; Korin, N.; Dinnar, U. Tunable Nonlinear Viscoelastic "Focusing" in a Microfluidic Device. *Phys. Rev. Lett.* **2007**, *98*, 234501.

(32) Asghari, M.; Serhatlioglu, M.; Ortaç, B.; Solmaz, M. E.; Elbuken, C. Sheathless Microflow Cytometry Using Viscoelastic Fluids. *Sci. Rep.* **2017**, *7*, 12342.

(33) Holzner, G.; Stavrakis, S.; deMello, A. Elasto-Inertial Focusing of Mammalian Cells and Bacteria Using Low Molecular, Low Viscosity PEO Solutions. *Anal. Chem.* **2017**, *89*, 11653−11663.

(34) Etcheverry, S.; Faridi, A.; Ramachandraiah, H.; Kumar, T.; Margulis, W.; Laurell, F.; Russom, A. High Performance Micro-Flow Cytometer Based on Optical Fibres. *Sci. Rep.* **2017**, *7*, 5628.

(35) Serhatlioglu, M.; Asghari, M.; Tahsin Guler, M.; Elbuken, C. Impedance-Based Viscoelastic Flow Cytometry. *Electrophoresis* **2019**, *40*, 906−913.

(36) Yuan, D.; Zhang, J.; Yan, S.; Peng, G.; Zhao, Q.; Alici, G.; Du, H.; Li, W. Investigation of Particle Lateral Migration in Sample-Sheath Flow of Viscoelastic Fluid and Newtonian Fluid. *Electrophoresis* **2016**, *37*, 2147−2155.

(37) Ha, B.; Park, J.; Destgeer, G.; Jung, J. H.; Sung, H. J. Transfer of Microparticles across Laminar Streams from Non-Newtonian to Newtonian Fluid. *Anal. Chem.* **2016**, *88*, 4205−4210.

(38) Nam, J.; Lim, H.; Kim, D.; Jung, H.; Shin, S. Continuous Separation of Microparticles in a Microfluidic Channel *via* the Elasto-Inertial Effect of Non-Newtonian Fluid. *Lab Chip* **2012**, *12*, 1347−1354.

(39) Lu, X.; Xuan, X. Elasto-Inertial Pinched Flow Fractionation for Continuous Shape-Based Particle Separation. *Anal. Chem.* **2015**, *87*, 11523−11530.

(40) Yang, S. H.; Lee, D. J.; Youn, J. R.; Song, Y. S. Multiple-Line Particle Focusing under Viscoelastic Flow in a Microfluidic Device. *Anal. Chem.* **2017**, *89*, 3639−3647.

(41) Zhou, Y.; Ma, Z.; Tayebi, M.; Ai, Y. Submicron Particle Focusing and Exosome Sorting by Wavy Microchannel Structures within Viscoelastic Fluids. *Anal. Chem.* **2019**, *91*, 4577−4584.

(42) Liu, C.; Zhao, J.; Tian, F.; Chang, J.; Zhang, W.; Sun, J. λ-DNA- and Aptamer-Mediated Sorting and Analysis of Extracellular Vesicles. *J. Am. Chem. Soc.* **2019**, *141*, 3817−3821.

(43) Tian, F.; Cai, L.; Chang, J.; Li, S.; Liu, C.; Li, T.; Sun, J. Label-Free Isolation of Rare Tumor Cells from Untreated Whole Blood by Interfacial Viscoelastic Microfluidics. *Lab Chip* **2018**, *18*, 3436−3445.

(44) Kang, K.; Lee, S. S.; Hyun, K.; Lee, S. J.; Kim, J. M. DNA-Based Highly Tunable Particle Focuser. *Nat. Commun.* **2013**, *4*, 2567.

(45) Seo, K. W.; Byeon, H. J.; Huh, H. K.; Lee, S. J. Particle Migration and Single-Line Particle Focusing in Microscale Pipe Flow of Viscoelastic Fluids. *RSC Adv.* **2014**, *4*, 3512−3520.

(46) Lim, E. J.; Ober, T. J.; Edd, J. F.; Desai, S. P.; Neal, D.; Bong, K. W.; Doyle, P. S.; McKinley, G. H.; Toner, M. Inertio-Elastic Focusing of Bioparticles in Microchannels at High Throughput. *Nat. Commun.* **2014**, *5*, 4120.

(47) Del Giudice, F.; Sathish, S.; D'Avino, G.; Shen, A. Q. From the Edge to the Center: Viscoelastic Migration of Particles and Cells in a

Strongly Shear-Thinning Liquid Flowing in a Microchannel. *Anal. Chem.* **2017**, *89*, 13146−13159.

(48) Lu, X.; Zhu, L.; Hua, R.; Xuan, X. Continuous Sheath-Free Separation of Particles by Shape in Viscoelastic Fluids. *Appl. Phys. Lett.* **2015**, *107*, 264102.

(49) Li, D.; Lu, X.; Xuan, X. Viscoelastic Separation of Particles by Size in Straight Rectangular Microchannels: A Parametric Study for a Refined Understanding. *Anal. Chem.* **2016**, *88*, 12303−12309.

(50) Young Kim, J.; Won Ahn, S.; Sik Lee, S.; Min Kim, J. Lateral Migration and Focusing of Colloidal Particles and DNA Molecules under Viscoelastic Flow. *Lab Chip* **2012**, *12*, 2807−2814.

(51) De Santo, I.; D'Avino, G.; Romeo, G.; Greco, F.; Netti, P. A.; Maffettone, P. L. Microfluidic Lagrangian Trap for Brownian Particles: Three-Dimensional Focusing down to the Nanoscale. *Phys. Rev. Appl.* **2014**, *2*, 064001.

(52) Liu, C.; Ding, B.; Xue, C.; Tian, Y.; Hu, G.; Sun, J. Sheathless Focusing and Separation of Diverse Nanoparticles in Viscoelastic Solutions with Minimized Shear Thinning. *Anal. Chem.* **2016**, *88*, 12547−12553.

(53) Liu, C.; Guo, J.; Tian, F.; Yang, N.; Yan, F.; Ding, Y.; Wei, J.; Hu, G.; Nie, G.; Sun, J. Field-Free Isolation of Exosomes from Extracellular Vesicles by Microfluidic Viscoelastic Flows. *ACS Nano* **2017**, *11*, 6968−6976.

(54) Dietsche, C.; Mutlu, B. R.; Edd, J. F.; Koumoutsakos, P.; Toner, M. Dynamic Particle Ordering in Oscillatory Inertial Microfluidics. *Microfluid. Nanofluid.* **2019**, *23*, 83.

(55) Mutlu, B. R.; Edd, J. F.; Toner, M. Oscillatory Inertial Focusing in Infinite Microchannels. *Proc. Natl. Acad. Sci. U. S. A.* **2018**, *115*, 7682−7687.

(56) Cruz, J.; Graells, T.; Walldén, M.; Hjort, K. Inertial Focusing with Sub-Micron Resolution for Separation of Bacteria. *Lab Chip* **2019**, *19*, 1257−1266.

(57) Decker, C. J.; Parker, R. P-bodies and Stress Granules: Possible Poles in the Control of Translation and mRNA Degradation. *Cold Spring Harbor Perspect. Biol.* **2012**, *4*, a012286.

(58) Sen, G. L.; Blau, H. M. Argonaute 2/RISC Resides in Sites of Mammalian MRNA Decay Known as Cytoplasmic Bodies. *Nat. Cell Biol.* **2005**, *7*, 633−636.

(59) Kowal, J.; Arras, G.; Colombo, M.; Jouve, M.; Morath, J. P.; Primdal-Bengtson, B.; Dingli, F.; Loew, D.; Tkach, M.; Théry, C. Proteomic Comparison Defines Novel Markers to Characterize Heterogeneous Populations of Extracellular Vesicle Subtypes. *Proc. Natl. Acad. Sci. U. S. A.* **2016**, *113*, E968−E977.

(60) Brunn, P. The Behavior of a Sphere in Non-Homogeneous Flows of a Viscoelastic Fluid. *Rheol. Acta* **1976**, *15*, 589−611.

(61) Naillon, A.; De Loubens, C.; Chèvremont, W.; Rouze, S.; Leonetti, M.; Bodiguel, H. Dynamics of Particle Migration in Confined Viscoelastic Poiseuille Flows. *Phys. Rev. Fluids* **2019**, *4*, 053301.

(62) Zęibacz, N.; Wieczorek, S. A.; Kalwarczyk, T.; Fiałkowski, M.; Hołyst, R. Crossover Regime for the Diffusion of Nanoparticles in Polyethylene Glycol Solutions: Influence of the Depletion Layer. *Soft Matter* **2011**, *7*, 7181−7186.

(63) Asghari, M.; Cao, X.; Mateescu, B.; van Leeuwen, D.; Stavrakis, S.; deMello, A. J. Oscillatory Viscoelastic Microfluidics for Efficient Focusing and Separation of Nanoscale Species. 2019, DOI: 10.1101/668301. bioRxiv. https://www.biorxiv.org/content/biorxiv/early/2019/06/13/668301.full.pdf (accessed Dec 1, 2019).